

# Experimental and ReaxFF-based molecular dynamics studies of the reaction of oxygen with DR-2 as a low global warming potential working fluid

Neng Tao<sup>1</sup>, Yuan Cheng<sup>1</sup>, Song Lu<sup>1</sup>, Haoran Xing<sup>1</sup>, Muhammad Shahid<sup>1</sup>, Siuming Lo<sup>2</sup>, and Heping Zhang<sup>1</sup>

<sup>1</sup>University of Science and Technology of China

<sup>2</sup>City University of Hong Kong

February 22, 2024

## Abstract

The *cis*-1,1,1,4,4,4-hexafluoro-2-butene (DR-2 or HFO-1336mzz(Z)) is a novel environmentally friendly working fluid with appropriate physicochemical characteristics. The present work firstly investigates decomposition mechanism and thermal stability of DR-2 under the atmosphere containing oxygen (O<sub>2</sub>) and high temperature experimentally. The oxidative degradation features of DR-2 were explored at the temperature of 473-1073 K and the products were monitored by GC-MS and IC. The experimental and ReaxFF-based molecular dynamics results demonstrated the promotion effects of O<sub>2</sub> on the DR-2 decomposition. The participation of O<sub>2</sub> molecules was supposed to lower the initial thermal decomposition temperature by 240 K approximately and also would increase the number of products such as hydrogen fluoride (HF), but the enhancement effect was weakened by the increasing reaction temperature. The reasonable Arrhenius parameters calculated from the first-order kinetic analyses-based reactive molecular dynamics (RMD) simulations. Combined with density functional theory, the pathways of initial oxidation decomposition product firstly observed in the experimental and RMD simulations were proposed in this study. These results may pave the way for further study of DR-2 as a working fluid with lower global warming potential.

1     **Experimental and ReaxFF-based molecular dynamics studies of the**  
2     **reaction of oxygen with DR-2 as a low global warming potential**  
3     **working fluid**

4     Neng Tao<sup>a</sup>, Yuan Cheng<sup>a</sup>, Song Lu<sup>a</sup>, Haoran Xing<sup>a</sup>, Muhammad Usman Shahid<sup>a</sup>, Siuming Lo<sup>b</sup>,  
5     Heping Zhang<sup>a,\*</sup>

6     <sup>a</sup> State Key Laboratory of Fire Science, University of Science of Technology of China, 230026, P.R.China.

7     <sup>b</sup> Department of Civil and Architectural Engineering, City University of Hong Kong, Tat Chee Avenue, Kowloon,  
8     Hong Kong

9     \*Corresponding author, Tel: (+86)551 63601665 ; Email address: zhanghp@ustc.edu.cn

10    **Abstract**

11        The cis-1,1,1,4,4,4-hexafluoro-2-butene (DR-2 or HFO-1336mzz(Z)) is a novel  
12    environmentally friendly working fluid with appropriate physicochemical  
13    characteristics. The present work firstly investigates decomposition mechanism and  
14    thermal stability of DR-2 under the atmosphere containing oxygen (O<sub>2</sub>) and high  
15    temperature experimentally. The oxidative degradation features of DR-2 were explored  
16    at the temperature of 473-1073 K and the products were monitored by GC-MS and IC.  
17    The experimental and ReaxFF-based molecular dynamics results demonstrated the  
18    promotion effects of O<sub>2</sub> on the DR-2 decomposition. The participation of O<sub>2</sub> molecules  
19    was supposed to lower the initial thermal decomposition temperature by 240 K  
20    approximately and also would increase the number of products such as hydrogen  
21    fluoride (HF), but the enhancement effect was weakened by the increasing reaction  
22    temperature. The reasonable Arrhenius parameters calculated from the first-order  
23    kinetic analyses-based reactive molecular dynamics (RMD) simulations. Combined  
24    with density functional theory, the pathways of initial oxidation decomposition product  
25    firstly observed in the experimental and RMD simulations were proposed in this study.  
26    These results may pave the way for further study of DR-2 as a working fluid with lower  
27    global warming potential.

28    **Keywords: ReaxFF MD; DR-2; DFT; oxidation thermal decomposition; HF**

## 29 1. Introduction

30 Due to the acceleration of the global warming, hydrocarbons with lower global  
31 warming potential (GWP) and zero ozone depletion potential (ODP) are of increasing  
32 interest nowadays [1]. As a novel working fluid with low GWP, DR-2, also  
33 abbreviated as HFO-1336mzz(Z), is one of the promising alternatives for HFC-245fa  
34 in the organic Rankine cycle (ORC) systems [2] and R134a in the Ejector Cooling  
35 Cycle systems [3]. In comparison with the first commercially available  
36 hydrofluoroolefins (HFOs) such as HFO-1234yf and HFO-1234ze-E, DR-2 shows the  
37 features of non-flammability at both 333 K and 373 K and chemical stability at high  
38 temperatures [4]. Moreover, DR-2 exhibited superior thermal properties to  
39 HCFO-1233zd (E) in the systems of ORC and vapor compression cycle [5]. Both the  
40 environmental friendliness and the extremely low acute toxicity of DR-2 will not  
41 cause irritation to human skin and eyes [6].

42 Previous studies mainly focused on the thermal stability, thermal decomposition  
43 mechanism and basic physical and chemical parameters of DR-2, and very  
44 meaningful results were obtained through experiments and theoretical calculations.  
45 Tao et al. [7] evaluated the production of hydrogen fluoride (HF) of pure DR-2 at  
46 873–1073 K in experiments. Huo et al. [8] studied the effect of pressure (2.1, 3.1 and  
47 4.0 MPa) on DR-2 for 24h, and the dissociation temperature was 583 K to 603 K, 563  
48 K to 583 K, and 543 K to 563 K, respectively. Huo et al. [9] investigated the pyrolysis  
49 process and product of DR-2 at 2000-3000 K with ReaxFF simulations, and the DR-2  
50 decomposition was divided into three phases. The same research group also discussed  
51 the impacts of copper (Cu), oxygen (O<sub>2</sub>), water (H<sub>2</sub>O) and polyol ester (POE)  
52 lubricants on the decomposition of DR-2 [10-13]. Except for a working fluid, DR-2  
53 was considered to be a promising fire extinguishing alternative for halon [14, 15].

54 The ReaxFF reaction force field was used to explore the complicated phenomena  
55 containing bond formation and breakage [16]. Therefore, the pyrolysis and oxidation  
56 decomposition of working fluids was extensively studied with ReaxFF simulation [11,

57 12, 17]. Moreover, the density functional theory (DFT) calculation was frequently  
58 conducted to investigate the chemical reactions of organic working fluids. Wang [18]  
59 et al. explored the further reaction of DR-2 products with active radicals such as OH·  
60 and H· radicals by DFT. Zhang [19] et al. reported the decomposition mechanism by  
61 DFT for the first time by studying the main pathways of the  $\text{CF}_3\text{CF}=\text{CH}_2$   
62 decomposition. Huang[20] et al. investigated the formation mechanisms of the main  
63 products ( $\text{CO}$ ,  $\text{CO}_2$  and  $\text{CH}_4$ ) in the thermal decomposition of lignin.

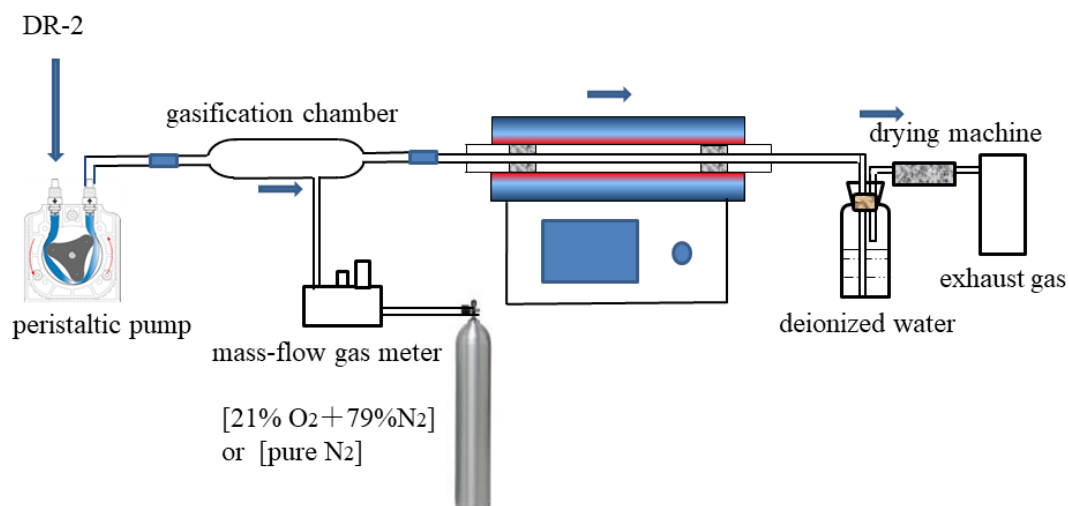
64 The heat sources are usually divided into both high-temperature and  
65 low-temperature heat sources according to different temperature ranges [1]. The  
66 working temperature of high-temperature heat sources can reach 873 K. At a higher  
67 operating temperature, the organic working fluid used in a supercritical ORC could be  
68 thermally decomposed, resulting in the changes in the thermal characteristics of the  
69 working fluid and the deviation of the parameters from the design conditions. The  
70 non-condensable gases and polymers produced from the thermal decomposition may  
71 cause the deterioration of heat transfer and blockage of the pipeline, which could lead  
72 to the safety problems in the ORC system. DR-2 was used as a working fluid with  
73 lower GWP in the ORC system for the experimental evaluation of micro-scale  
74 cryogenic applications[21]. Thus, it is of great importance to study its thermal  
75 decomposition features under high temperature and oxygen-containing conditions.  
76 Although the physicochemical properties of DR-2 have been extensively reported, its  
77 thermal decomposition products in the presence of  $\text{O}_2$  at high temperatures are still  
78 unclear.

79 In this study, we investigate the initial decomposition temperature, main product  
80 such as HF and the related kinetics of DR-2 in the presence of  $\text{O}_2$  experimentally and  
81 RMD simulations under high temperature. It is expected to benefit the environment  
82 protection and the industry application security of DR-2.

## 83 2. Methodologies

### 84 2.1 Experimental apparatus and procedures

85 In the experimental system (Fig 1), the pyrolysis process of DR-2 was studied in  
86 the atmospheres of two gases (pure N<sub>2</sub> and synthetic air) from 473 to 1073 K. The  
87 CF<sub>3</sub>CH=CHCF<sub>3</sub> with a purity of above 99.5% (Kemu Fluoride Technology Co., Ltd.)  
88 was used directly without purification. The nitrogen with a purity of above 99.99%  
89 and the synthetic air with a composition of 21% O<sub>2</sub> and 79% N<sub>2</sub> employed in the  
90 experiments were provided by the local commercial suppliers. Prior to the thermal  
91 degradation experiment, the preheating of each quartz tube was conducted at 1123 K  
92 under argon flow for 1 h. The argon gas (purity  $\geq$ 99.99%) was used to purge the  
93 impurity gases in the experimental pipeline. The gasification of pure DR-2(l) was  
94 realized by preheating it to 343 K. At the same time, the reactor temperature was set  
95 to 473-1073 K with a constant temperature zone length of 225 mm ( $\pm$ 5 K). The quartz  
96 tube in the tube furnace could be replaced with a new one at a varying decomposition  
97 temperature. The length and inner diameter of the quartz tubular reactor were 1100  
98 mm and 10 mm, respectively. In the experiment, the temperature of the furnace was  
99 set to 473-973 K with an interval of 100 K and 973-1073 K with an interval of 20 K,  
100 respectively. After the temperature was kept at the above-mentioned set points for 2 h,  
101 the vaporization setup was heated with a peristaltic pump flow rate of 0.41 mL/min  
102 and a mass flowmeter value of 100 mL/min. The pyrolysis time was 0.5 h. The  
103 thermal degradation products of DR-2 were collected by the gas-collecting pockets  
104 and 400 mL of deionized water. Finally, the exhaust gases at the end of the experiment  
105 were disposed by sodium hydroxide (NaOH) aqueous solution before discharge. The  
106 fluoride concentration in the solution was measured by the ion chromatography (IC)  
107 after the adsorption of gas products in 400 mL of deionized water. Finally, the exhaust  
108 gases were analyzed by GC-MS.



109

110

**Fig 1.** Scheme of the DR-2 oxidation pyrolysis system.

## 111 2.2 ReaxFF MD simulations

112 Although part of the thermal decomposition products was detected in the thermal  
 113 decomposition experiment, the intermediate products and the product formation  
 114 mechanism are still unknown. The quantum chemistry calculation by the simulation  
 115 method of ReaxFF-MD could be in good consistence with corresponding  
 116 experimental results. This method was widely used in various reaction systems, such  
 117 as the thermal decomposition of fossil fuels, the oxidation or combustion processes of  
 118 alkanes and hydrocarbons, and the explosion of energetic materials [17, 22-24]. The  
 119 bond formation and breakage in the molecular dynamic simulation could be described  
 120 by ReaxFF, a reactive force field based on the bond order firstly proposed by van  
 121 Duin [25, 26].

122 The ReaxFF energy function was expressed by Equation (1).

$$123 \quad E_{system} = E_{bond} + E_{over} + E_{under} + E_{val} + E_{pen} + E_{tors} + E_{conj} +$$

$$124 \quad E_{vdWaals} + E_{Coulomb} \quad (1)$$

125 Where  $E_{bond}$  is the bond energy,  $E_{over}$  is the over-coordinated atom in the  
 126 molecular energy contribution (MEC),  $E_{under}$  is the under-coordinated atom in the  
 127 MEC,  $E_{val}$  is the valence angle terms,  $E_{pen}$  is the penalty energy,  $E_{tors}$  is the

128 torsion energy,  $E_{conj}$  is the conjugation effects in the energy contribution,  $E_{vdWaals}$   
129 is the non-bonded van der Waals interactions, and  $E_{Coulomb}$  is the non-bonded  
130 Coulomb interactions.

131 In order to accelerate the reaction speed within the simulation time range, the  
132 simulation temperature range was set to 1000-3400 K (higher than experimental  
133 temperature in this work) to study the pyrolysis mechanism of DR-2. In a reasonable  
134 time, the simulated temperature should be higher than the actual temperature in  
135 average to speed up the dynamic simulation of the activation process [27, 28].  
136 According to Arrhenius equation [29], temperature will only change the reaction rate  
137 to a certain extent, but will not change the reaction path.

### 138 2.3 Density functional theory (DFT) calculations

139 To investigate the initiation mechanism of DR-2 oxidation and dissociation, the  
140 DFT approach was used to compute the initial reaction energy barriers based on the  
141 products of the experimental results. By the B3LYP method, based on 6-311 ++ G (d,  
142 p), the reactant geometric structure, the transition state and the initial decomposition  
143 pathway were optimized at 298 K and 0.1 MPa. The Gaussian 09 suite of programs  
144 was employed for the calculation of all the reactions [30].

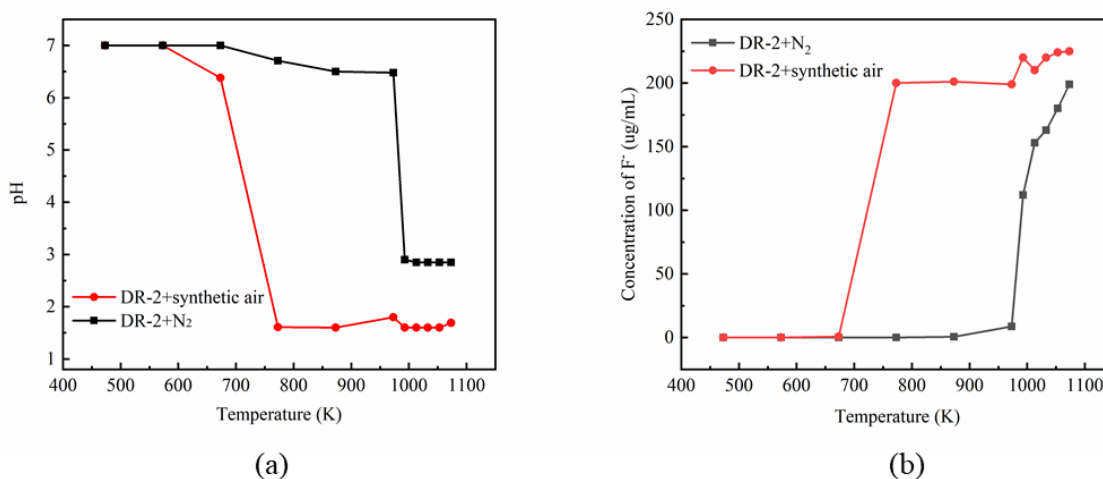
## 145 3. Results and discussion

### 146 3.1 Experimental Section

#### 147 3.1.1 The Trend of Hydrogen Fluoride Concentration

148 Due to the toxicity of HF, it is noteworthy of monitoring the content variation of  
149 HF generated during the DR-2 decomposition. The gradual increases in the hydrogen  
150 ion concentration ( $[H^+]$ ) and the fluoride ion concentration ( $[F^-]$ ) were accompanied  
151 by the increasing pyrolysis temperature (473-1033 K), and the tendency of increase  
152 was finally stabilized (Fig. 2). Under different gas atmospheres, drastic changes in  $[H^+]$

153 and  $[F^-]$  were observed at varying temperatures. In the pure nitrogen atmosphere,  
 154 great changes in the pH and  $[F^-]$  of the solution were seen due to the absorption of the  
 155 thermal decomposition products at 1013 K. However, in the atmosphere of synthetic  
 156 air, the sharp concentration variations were found at 773 K. Obviously, the amount of  
 157 HF produced in synthetic air was higher than that in pure  $N_2$ . Thus, the presence of  $O_2$   
 158 would facilitate the DR-2 decomposition. On the one hand,  $O_2$  would lower the  
 159 degradation temperature of DR-2 from 1013 K to 773 K. On the other hand, the  
 160 increased HF content generated under oxygen-containing conditions would enhance  
 161 the thermal decomposition degree of DR-2. When the temperature reached a certain  
 162 level, the decomposition rate of DR-2 would quickly change, but the effect of  
 163 increasing the temperature on thermal decomposition would weaken or disappear. It is  
 164 easy to find that the pH value remains unchanged when a certain temperature is  
 165 reached, but the fluoride ion concentration ( $[F^-]$ ) continues to increase, because the  
 166 deionized water also absorbs other fluorine-containing products. This would result in  
 167 a lower concentration of HF released from the experiment, since the silicon  
 168 tetrafluoride was detected on the surface of the reaction quartz tube.

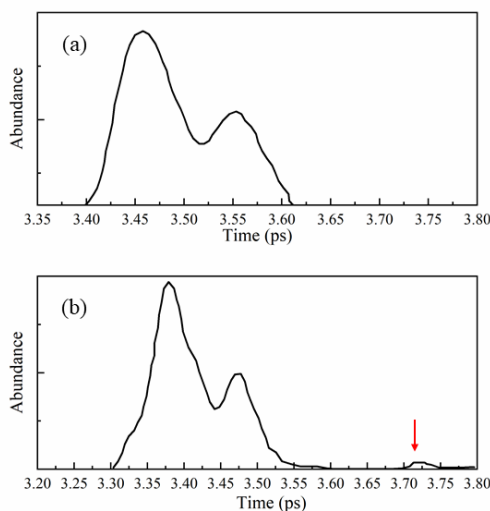


169 **Fig 2.** The change of pH and  $[F^-]$  formed in the DR-2 decomposition at different temperatures.

### 170 3.1.2 GC-MS analyses of the gaseous products

171 The gaseous products generated by the oxidation thermal decomposition were

172 collected in the solution. The DR-2 oxidation products were identified by the GC-MS  
 173 method. Two main peaks were seen in the GS-MS analysis (Fig. 3), indicating the  
 174 undecomposed synthetic air and DR-2 in the collected gases. Upon higher thermal  
 175 decomposition temperature, a small peak in Fig. 3 (b) was observed, which was  
 176 identified as  $C_4H_2OF_6$  based on the standard mass spectrum library.



177  
 178 **Fig 3.** GC-MS results of the exhaust gas of DR-2 oxidation Pyrolysis  
 179 (a: 673 K; b: 1103 K)

### 180 3.2 ReaxFF-MD simulation

181 To simulate the actual conditions, the initial densities of the system containing  
 182 DR-2 and  $O_2$  were set as  $1.36 \text{ g cm}^{-3}$  (the actual liquid density at 300 K and 0.1 MPa)  
 183 and  $0.00538 \text{ g cm}^{-3}$  (the actual vapor density at 300 K and 0.1 MPa) [5]. Therefore,  
 184 the initial densities of the system containing DR-2 set in this work were of great  
 185 importance. Such densities in previous work was  $1.3595$  and  $0.015 \text{ g cm}^{-3}$  (Table 1).

186 **Table 1**

187 Initial densities and ensemble of ReaxFF simulation about DR-2.

	Molecules	Initial density ( $\rho/\text{g} \cdot \text{cm}^{-3}$ )	Ensemble
Ref.[9]	50 DR-2	1.3595	NVT
Ref.[11]	150 DR-2 + 450 $O_2$ (1)	0.015 (1)	NVT
	75 DR-2 + 450 $O_2$ (2)		
	300 DR-2 + 450 $O_2$ (3)		

	150 DR-2 + 450 O <sub>2</sub> (1)		
	150 DR-2 + 450 O <sub>2</sub> +37 H <sub>2</sub> O (2)		
Ref.[12]	150 DR-2 + 450 O <sub>2</sub> +75 H <sub>2</sub> O (3)	0.015	NVT
	150 DR-2 + 450 O <sub>2</sub> +112 H <sub>2</sub> O (4)		
	150 DR-2 + 450 O <sub>2</sub> +150 H <sub>2</sub> O (5)		
	100 DR-2 + 50 O <sub>2</sub> (1)		
This work	45 DR-2 (2)	0.00538 (1)	NVT
	45 DR-2 +5 O <sub>2</sub> (3)	1.36 (2-3)	

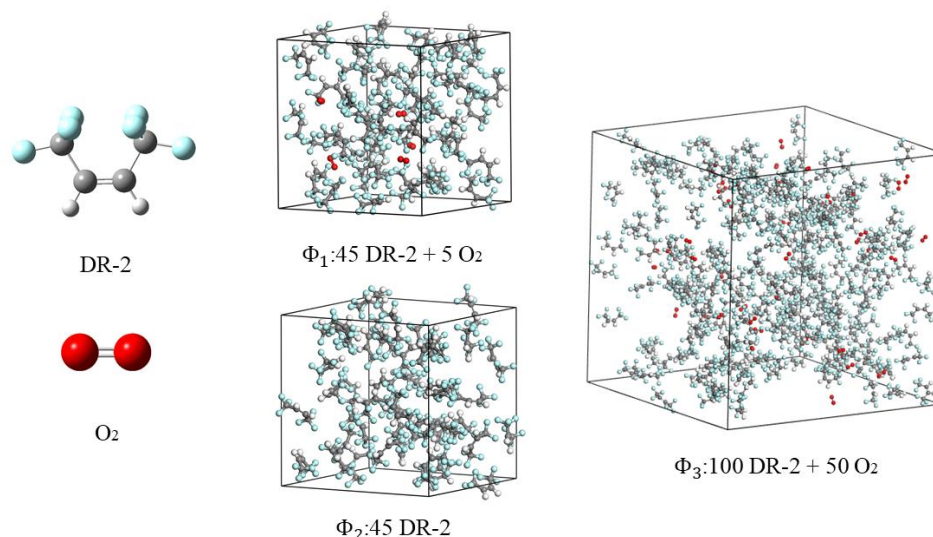
188 To understand the pyrolysis process induced by the temperature, the RMD  
189 simulations at varying temperatures were carried out on the pure DR-2 system and the  
190 system including DR-2 and O<sub>2</sub> for the first time. The pure 45 DR-2 or 45 DR-2 and 5  
191 O<sub>2</sub> were placed in two periodic boxes measuring 20.81 Å × 20.81 Å × 20.81 Å ( $\Phi_1$ )  
192 and 20.96 Å × 20.96 Å × 20.96 Å ( $\Phi_2$ ) with a system density of 1.36 g · cm<sup>-3</sup> (Fig.  
193 4). The system  $\Phi_1$  and  $\Phi_2$  were first minimized via MD at a low temperature (5 K)  
194 with the NVT ensemble and then were equilibrated with the NVT ensemble for 50 ps  
195 at 300 K using a time step of 0.1 fs. The temperature was elevated from 1000 K to  
196 3400 K with a ramp of 9.6 K·ps<sup>-1</sup> for 250 ps, followed by maintaining for 50 ps at  
197 3400 K.

198 To study the kinetic analysis of the pure DR-2 and the system containing DR-2  
199 and O<sub>2</sub> at elevated temperatures, the RMD simulations were employed with NVT  
200 (constant particle number, constant volume, and constant temperature) ensemble at  
201 2600-3400 K with an interval of 200 K and a reaction time of 100 ps. Prior to the  
202 desired RMD simulations, the systems  $\Phi_1$  and  $\Phi_2$  were equilibrated for 50 ps  
203 (picosecond) at 300 K.

204 To study the pyrolysis product distribution of the system including DR-2 and O<sub>2</sub>,  
205 the oxidation decomposition process was analyzed by the RMD simulations. The 100  
206 DR-2 and 50 O<sub>2</sub> were placed in unit cells and the molecules structure were optimized  
207 (Fig. 4). The sides of unit cells were 177.11 Å × 177.11 Å × 177.11 Å ( $\Phi_3$ ) with a  
208 density of 0.00538 g · cm<sup>-3</sup>.

209 For all the ReaxFF simulations, the ReaxFF parameters [31] for C, H, O and F  
210 atoms were adopted in this work. Recent studies [11, 12] used in this ReaxFF

211 parameters have revealed that the outcomes at high temperatures of ReaxFF MD  
212 simulations on DR-2 were in good agreement with those of experiments [14, 18]. And  
213 the reaction temperature was adjusted by a Berendsen thermostat with a damping  
214 constant of 200 fs.

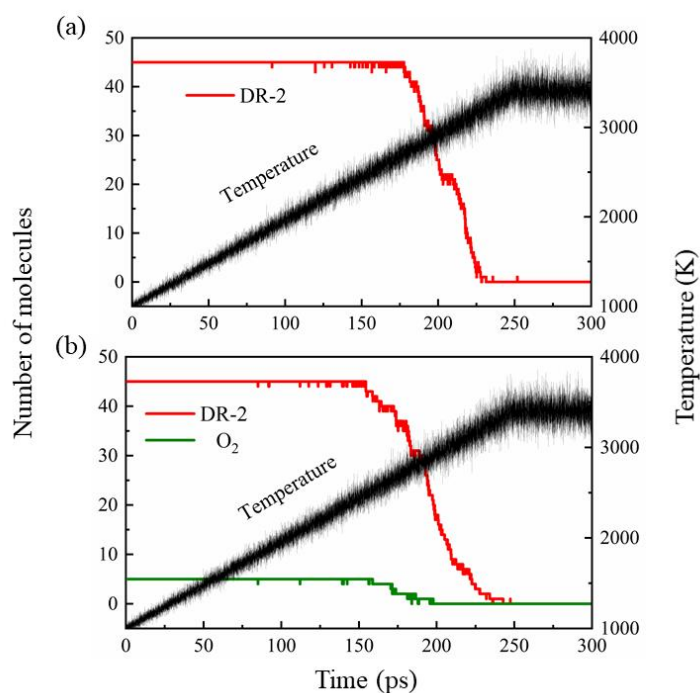


215  
216 **Fig 4.** The snapshots of optimized molecular structure and the equilibrated unit cells of the DR-2  
217 with O<sub>2</sub>  
218 (The colors of gray, white, red, and blue spheres represented the C, H, O, and F atoms,  
219 respectively.)

### 220 3.2.1 Initial decomposition temperature and kinetic analysis of DR-2 (liquid) 221 decomposition in the absence and presence of O<sub>2</sub>

222 To obtain the initial decomposition temperature of DR-2 (liquid), the RMD  
223 simulations in the absence and presence of O<sub>2</sub> were conducted at the temperature of  
224 1000-3400 K and a density of 1.36 g·cm<sup>-3</sup>. Clearly, the initial dissociation  
225 temperature of pure DR-2 was about 2713 K at 178 ps (Fig. 5(a)), and the DR-2 in the  
226 presence of O<sub>2</sub> began to decompose at 2484 K and a time of 178 ps (Fig. 5(b))  
227 approximately. The initial degradation temperature of DR-2 was reduced from 2723 K  
228 to 2484 K in the presence of O<sub>2</sub> molecules. It also can be found that DR-2 and O<sub>2</sub>  
229 molecules start to dissociate almost simultaneously. When the temperature reaches

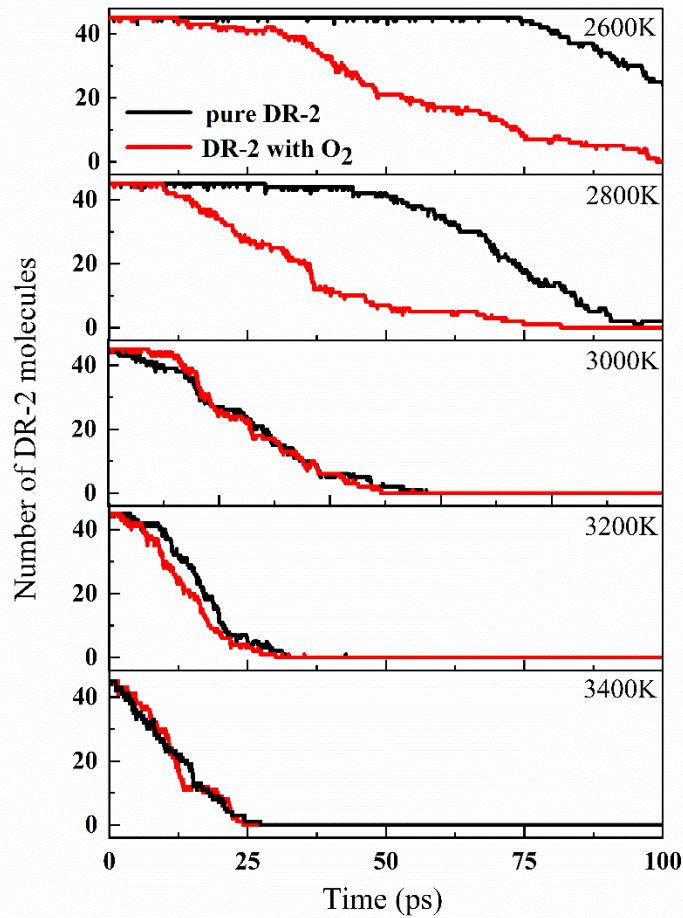
230 3400 K, the reactant molecules would be consumed completely



231

232 **Fig 5.** The time evolutions of the DR-2 (a) in the absence and (b) presence of O<sub>2</sub> at a density of  
233 1.36 g·cm<sup>-3</sup> and a temperature of 2600-3400K in RMD simulation

234 According to the consumption rate and the initial decomposition temperature of  
235 DR-2 in Fig. 5, the temperature-dependent NVT-MD simulations were carried out for  
236 kinetic analysis of the DR-2 degradation in the absence and presence of O<sub>2</sub> at 100 ps  
237 and a temperature of 2600-3400 K with an interval of 200 K. The increasing  
238 temperature was accompanied by the obvious increase of decomposition rates of  
239 DR-2 (Fig. 6). In addition, the dissociation of DR-2 was especially accelerated by 5  
240 O<sub>2</sub> molecules at lower temperatures of 2600 K and 2800 K, and this impact became  
241 insignificant at the temperature higher than 3000 K. Because the high energy  
242 self-dissociation pathway became accessible for DR-2 when the temperature up to  
243 3000K. At the same time, the presence of O<sub>2</sub> molecules became insignificant at higher  
244 temperature.



245

246

247

248

249

250

251

252

253

254

255

256

257

258

259

**Fig 6.** Comparison of time evolutions of DR-2 in the absence and presence O<sub>2</sub> in NVT-MD simulation at a density of 1.36 g·cm<sup>-3</sup> at 2600K, 2800k, 3000K,3200K and 3400K, respectively.

The rate constant  $k$  at each temperature was calculated by the relation of the number of DR-2 molecules over time through first-order kinetics:

$$\ln N_t - \ln N_0 = -kt \quad (2)$$

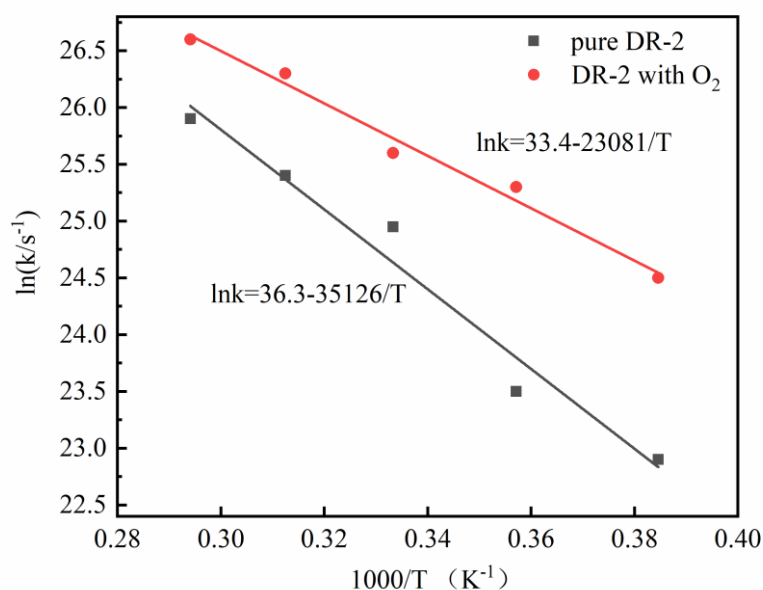
where  $N_0$  and  $N_t$  are the number of DR-2 molecules at the beginning and at time  $t$ , respectively.

$$\ln k = \ln A - E_a/Rt \quad (3)$$

where  $R$  is the universal gas constant and  $T$  is the pyrolysis temperature. The fitted Arrhenius plot of the DR-2 decomposition process in the absence and presence of O<sub>2</sub> were shown in Fig. 7. The activation energy ( $E_a$ ) of thermal decomposition of DR-2 in the presence of O<sub>2</sub> was calculated to be about 191.9 kJ/mol, being about 100 kJ/mol lower than that for pure DR-2.

Based on the effect of O<sub>2</sub> molecules on the initial decomposition temperature and

260 kinetics during the DR-2 degradation, the DR-2 decomposition could be strongly  
261 promoted by a small amount of O<sub>2</sub> molecules at high temperatures in a liquid state.  
262 Thus, it was of great significance to exclude O<sub>2</sub> or air when DR-2 was acted as a  
263 high-temperature working fluid. However, there is no experimental data on liquid  
264 DR-2 decomposition with O<sub>2</sub> currently and the relevant experiments are needed to  
265 compare with the theoretical results in this work for future research.



266

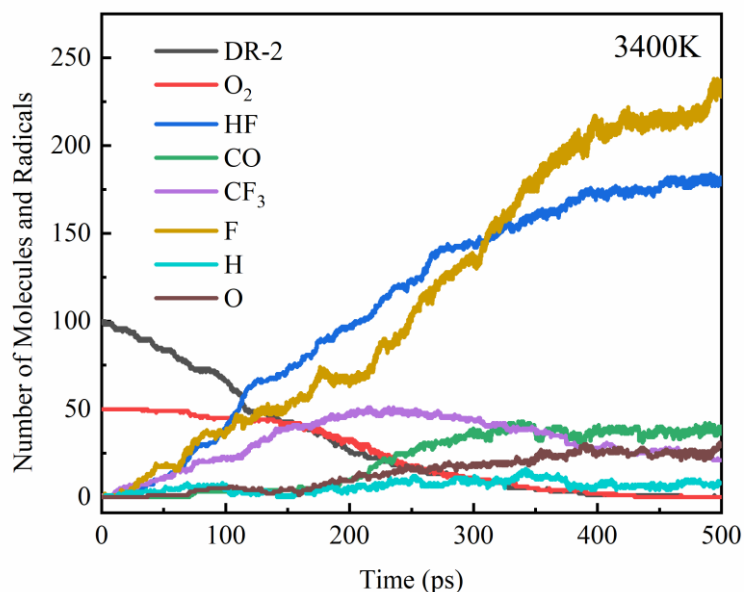
267 **Fig 7.** The fitted rate constant versus temperature (2600-3400 K) obtained from 100 ps  
268 NVT-RMD simulations at a density of 1.36 g·cm<sup>-3</sup> of DR-2 pyrolysis in the absence and presence  
269 of O<sub>2</sub>.

### 270 3.2.2 Temperature effects on DR-2 (vaporous) decomposition in presence of O<sub>2</sub>

271 By considering the amounts of synthetic air and DR-2 in our experiment and  
272 the vapor density of DR-2 (0.00538 g cm<sup>-3</sup>) at 300 K and 0.1 Mpa, a series of ReaxFF  
273 simulations were conducted with NVT ensemble at 2600 K, 2800 K, 3000 K, 3200 K  
274 and 3400 K and a reaction time of 500 ps to obtain the oxidation process and products  
275 of DR-2.

276 The oxidation dissociation process of  $\Phi_3$  for 500 ps at 3400 K was  
277 investigated (Fig. 8). Clearly, HF and CO were the main products of thermal

278 decomposition of DR-2. The thermal degradation process of the system could be  
279 divided into 3 phases. In the first stage (0-175 ps), the consumption of oxygen  
280 molecules was relatively low, and DR-2 molecules underwent self-thermal  
281 decomposition to produce radicals. In the second phase (175-325 ps), the number of  
282 O<sub>2</sub> was equal to that of DR-2 molecules at the beginning. The collision of radicals and  
283 O<sub>2</sub> molecules with DR-2 resulted in the decomposition and final consumption of  
284 DR-2 together with O<sub>2</sub>. The number of CF<sub>3</sub> radicals was increased up to the maximum  
285 value, followed by the slow consumption. The reaction of O<sub>2</sub> with DR-2 molecules  
286 was accompanied by the breakage of the C-F bond and the production of more F  
287 radicals. The CO molecules and O radicals reached their maximum values at this stage  
288 as the thermal decomposition continued. In the third stage (325-500 ps), the numbers  
289 of HF and F were increased to the maximum.



290

291

**Fig 8.** The oxidation decomposition of DR-2 at 3400K

292

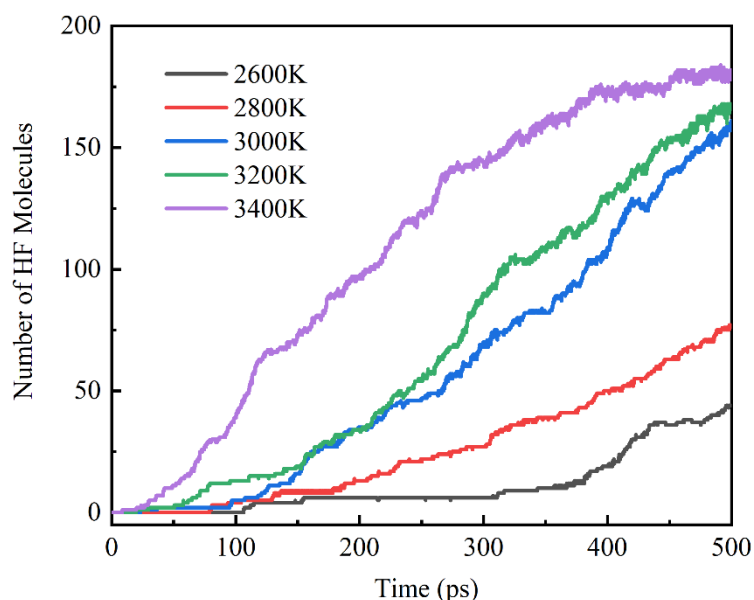
293

294

295

In RMD simulations and experiments, HF was obviously the main product of the oxidative decomposition reaction of DR-2. The evolution of the number of HF at 2600-3400 K over the time in the ReaxFF simulations was studied (Fig. 9). The increasing temperature was accompanied by the obviously increasing amount of HF.

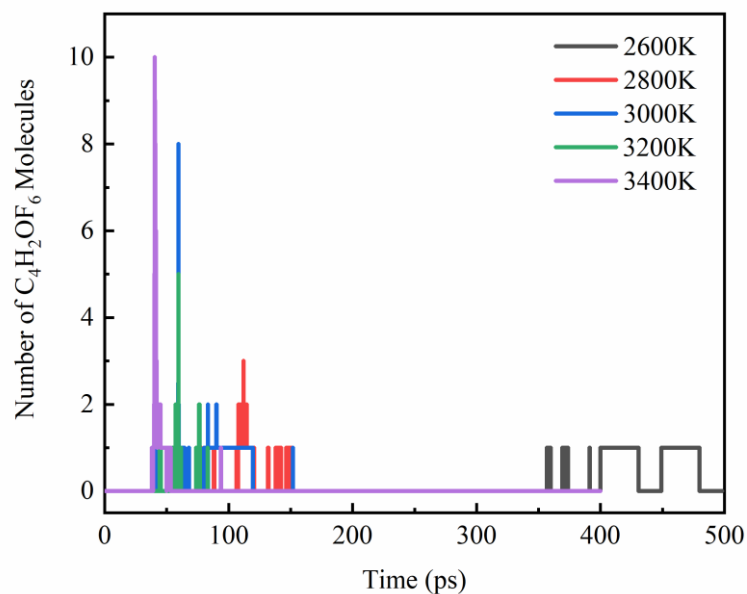
296 At 3000 K, the number of HF molecules was increased by 2-3 times. This  
297 phenomenon was consistent with previous experiment. At the temperature of 2600 K,  
298 the production of HF occurred at around 300 ps and reached around 40 at 500 ps. At  
299 the temperature of 2800 K, the time for the production of HF was advanced, and  
300 finally the production reached about 60. At 3000-3400 K, the HF generation rate was  
301 significantly improved, and the final HF amount was 150-200. At this time, the  
302 increase in temperature demonstrated a small effect on the production of HF. This was  
303 consistent with the experimental results.



304

305 **Fig 9.** The evolution of the HF production at different temperatures over time

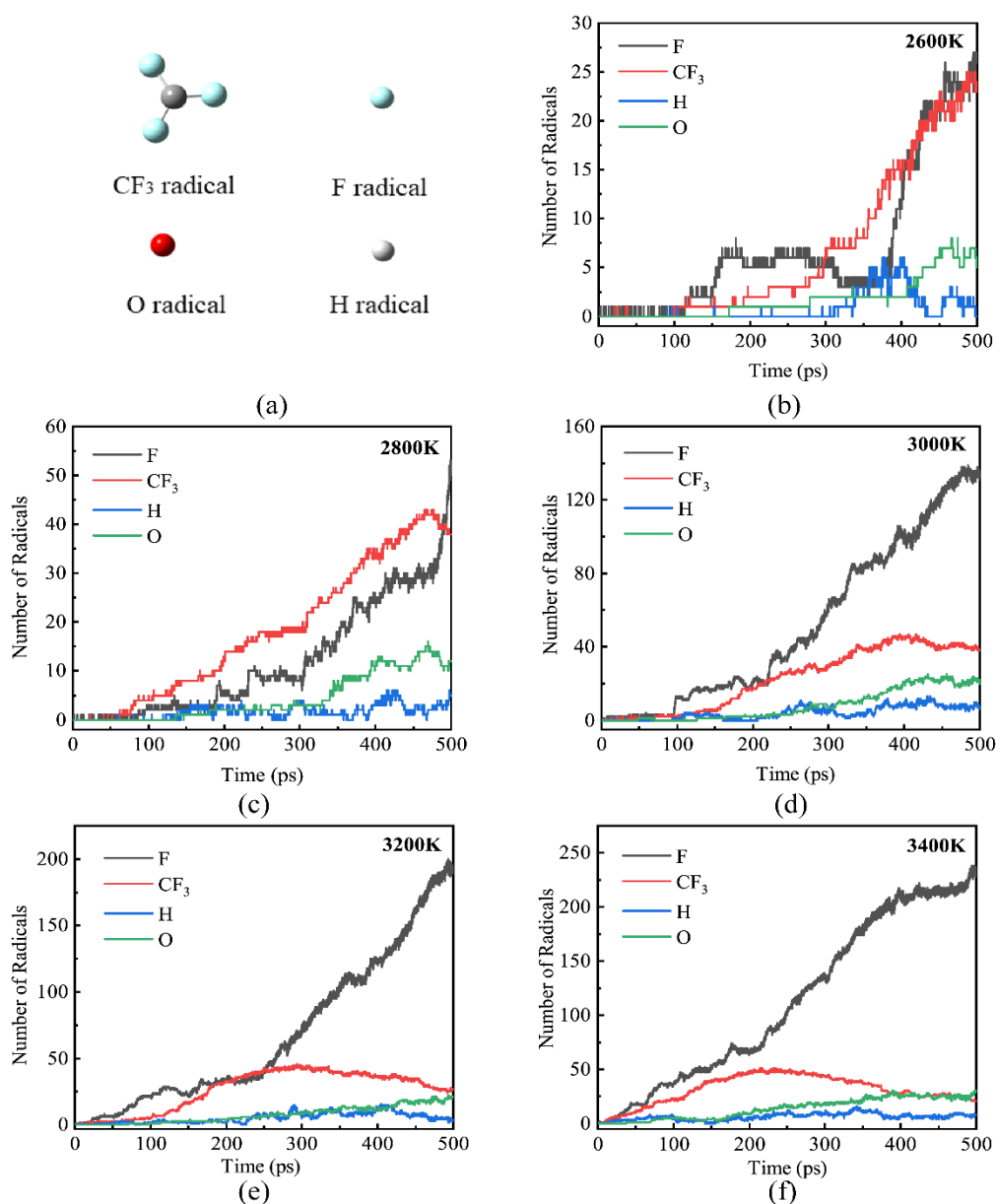
306 As detected to be the principal product by GC-MS in Section 3.1,  
307  $\text{CF}_3\text{CHOCHCF}_3$  was also found in the ReaxFF-MD simulation at 2600-3400 K (Fig.  
308 10). At 2600 K, the production of  $\text{CF}_3\text{CHOCHCF}_3$  molecule occurred at 350-500 ps  
309 and the number of the molecule was just one. At 2800-3400 K, the production of  
310  $\text{CF}_3\text{CHOCHCF}_3$  molecule occurred at 50-150 ps and the number of this molecule was  
311 just 1-10. Thus, the  $\text{CF}_3\text{CHOCHCF}_3$  molecule was an intermediate and its residence  
312 time in the system was relatively short.



313

314 **Fig 10.** The evolution of the number of  $C_4H_2OF_6$  molecule at different temperatures over  
 315 time

316 The radicals were generated during the collision reaction between  $O_2$  and DR-2  
 317 and the DR-2 self-decomposition, thereby promoting the completion of the reaction.  
 318 The evolution of the number of small radicals containing F,  $CF_3$ , H and O radicals at  
 319 different temperatures over time was shown in Fig. 11. The constant increase of the F  
 320 radical number was accompanied by the rising temperature. At lower temperatures of  
 321 2600 K and 2800 K, the continuous increase in  $CF_3$  radicals and F radicals was  
 322 observed over time, and the final production amounts were equivalent. However, at  
 323 3000-3400 K, the increase in the number of  $CF_3$  radicals was followed by a decrease,  
 324 and the time to reach the maximum was continuously shortened. The numbers of O  
 325 and H radicals were less in the whole reaction.



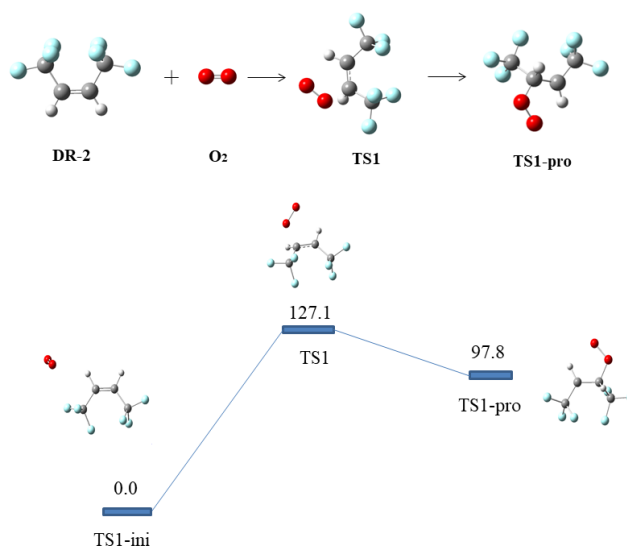
326  
327  
328  
329

**Fig 11.** The evolution of the number of small radicals at different temperatures over time (The colors of gray, white, red, and blue spheres represented the C, H, O, and F atoms, respectively.)

### 330 3.3 Initiation oxidation decomposition reactions of DR-2

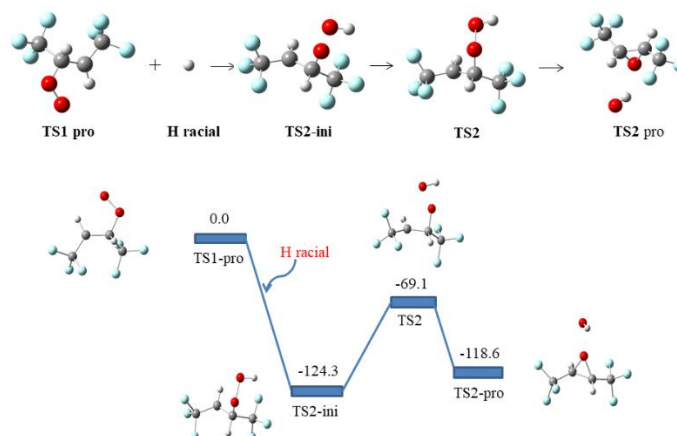
331 In both the experimental and the ReaxFF simulation parts, extremely lower  
332 content of  $\text{CF}_3\text{CHOCHCF}_3$  was found than HF, indicating that it may be an  
333 intermediate product of the oxidation thermal decomposition of DR-2. The DFT  
334 approach was used to compute the formation process and energy barrier of

335  $\text{CF}_3\text{CHOCHCF}_3$ . The  $\text{O}_2$  molecules attacked C atoms in  $\text{C}=\text{C}$  bonds, forming TS1  
 336 with an energy barrier of 127.1 kJ/mol (Fig. 12). This energy barrier was lower than  
 337 the bond dissociation energy of DR-2, so the  $\text{O}_2$  molecule could promote the  
 338 decomposition of DR-2 at high temperatures. As described in the ReaxFF simulation,  
 339 the self-oxidative decomposition of DR-2 may generate  $\text{CF}_3$ , F, H and O radicals. For  
 340 example, the H radical oxidative thermal decomposition system would react with  
 341 TS1-pro and form TS2-pro (OH radical and  $\text{CF}_3\text{CHOCHCF}_3$ ) and release 124.3  
 342 kJ/mol, implying the promotion effect of H radical on the progress of the reaction (Fig.  
 343 13). Meanwhile, the  $\text{CF}_3$ , F and O radicals also would react with TS1-pro to form  
 344  $\text{CF}_3\text{CHOCHCF}_3$ .



345

346 **Fig 12.** The proposed pathways and energy profiles of the collision of between oxygen and DR-2  
 347 (The colors of gray, white, red, and blue spheres represented the atoms of C, H, O, and F,  
 348 respectively.)



349

350 **Fig 13.** The proposed pathways and energy profiles of DR-2 and H radical  
351 (The colors of gray, white, red, and blue spheres represented the atoms of C, H, O, and F,  
352 respectively.)

#### 353 **4. Conclusion**

354 The oxidation thermal decomposition of DR-2 was investigated experimentally  
355 and theoretically at high temperature in this study. The experimental investigated  
356 main DR-2 decomposition products under high temperature (from 473K to 1073K) in  
357 a tubular reactor detected by IC and GC-MS. A series of the reactive molecule  
358 dynamics (RMD) simulations were conducted to figure out the effect of O<sub>2</sub> molecules  
359 on the decomposition of DR-2 at liquid and vaporous state. The possible pathways of  
360 the initial decomposition products of C<sub>4</sub>H<sub>2</sub>OF<sub>6</sub> were proposed by DFT method. The  
361 conclusions can be summarized as follows:

362 (1) The promoting effect of O<sub>2</sub> molecules on DR-2 was manifested in two  
363 aspects. The thermal decomposition degree and decomposition products such as HF  
364 increased by lowering the initial thermal decomposition temperature of DR-2 (from  
365 993 K to 673 K). However, this promoting effect would be weakened when a certain  
366 temperature was reached.

367 (2) HF was one of the main products of thermal decomposition of DR-2 with O<sub>2</sub>  
368 under high temperature, and the ReaxFF MD simulation were in good agreement with  
369 the experimental results.

370 (3) The activation energy (E<sub>a</sub>) of thermal decomposition of DR-2 in the presence  
371 of O<sub>2</sub> was calculated from RMD simulations based on kinetic analysis to be about  
372 191.9 kJ/mol, being 100 kJ/mol lower than that for pure DR-2 approximately.

373 (4) Both the GC-MS and ReaxFF MD simulation results detected the oxidation  
374 product of the double bond in DR-2, and the process of O<sub>2</sub> molecule attacking DR-2  
375 to form the oxidation products was deduced in combination with the DFT method.

376

377

378 **Acknowledgments**

379       The quantum chemical calculations were conducted through ADF software and  
380 the supercomputing system at State Key Laboratory of Fire Science of USTC.

381

382

383

384

385

386

387

388

389

390

391

392

393

394

395

396

397

398

399

400

401

402

403

404 **References**

- 405 1. Moles, F., et al., *Thermo-economic evaluation of low global warming potential*  
406 *alternatives to HFC-245fa in Organic Rankine Cycles*. Energy Procedia, 2017.  
407 **142**: p. 1199-205.
- 408 2. Moles, F., et al., *Thermo-economic evaluation of low global warming potential*  
409 *alternatives to HFC-245fa in Organic Rankine Cycles*, in *Proceedings of the 9th*  
410 *International Conference on Applied Energy*, J. Yan, J. Wu, and H. Li, Editors.  
411 2017. p. 1199-1205.
- 412 3. Gil, B. and J. Kasperski, *Efficiency Evaluation of the Ejector Cooling Cycle*  
413 *using a New Generation of HFO/HCFO Refrigerant as a R134a Replacement*.  
414 Energies, 2018. **11**(8).
- 415 4. Kontomaris, K., *HFO-1336mzz-Z: High Temperature Chemical Stability and*  
416 *Use as A Working Fluid in Organic Rankine Cycles*. International Refrigeration  
417 and Air Conditioning Conference, 2014b: p. 1525.
- 418 5. Moles, F., et al., *Low GWP alternatives to HFC-245fa in Organic Rankine*  
419 *Cycles for low temperature heat recovery: HCFO-1233zd-E and*  
420 *HFO-1336mzz-Z*. Applied Thermal Engineering, 2014. **71**(1): p. 204-212.
- 421 6. *Cis-1,1,1,4,4,4-hexafluoro-2-butene (HFO-1336mzz-Z) (2018)*. Toxicology and  
422 industrial health, 2019: p. 748233719825530.
- 423 7. Tao, N., et al., *Experimental and Density Functional Theory Studies on*  
424 *1,1,1,4,4,4-Hexafluoro-2-Butene Pyrolysis*. Molecules (Basel, Switzerland),  
425 2020. **25**(17).
- 426 8. Huo, E.G., et al., *Thermal stability and decomposition mechanism of*  
427 *HFO-1336mzz(Z) as an environmental friendly working fluid: Experimental*  
428 *and theoretical study*. International Journal of Energy Research, 2019. **43**(9): p.  
429 4630-4643.
- 430 9. Huo, E.G., et al., *A ReaxFF-based molecular dynamics study of the pyrolysis*  
431 *mechanism of HFO-1336mzz(Z)*. International Journal of Refrigeration-Revue  
432 Internationale Du Froid, 2017. **83**: p. 118-130.
- 433 10. Huo, E., et al., *Dissociation mechanisms of HFO-1336mzz(Z) on Cu(111),*  
434 *Cu(110) and Cu(100) surfaces: A density functional theory study*. Applied  
435 Surface Science, 2018. **443**: p. 389-400.
- 436 11. Huo, E., et al., *A ReaxFF-based molecular dynamics study of the oxidation*  
437 *decomposition mechanism of HFO-1336mzz(Z)*. International Journal of  
438 Refrigeration-Revue Internationale Du Froid, 2018. **93**: p. 249-258.
- 439 12. Huo, E.G., et al., *The oxidation decomposition mechanisms of HFO-1336mzz(Z)*  
440 *as an environmentally friendly refrigerant in O-2/H2O environment*. Energy,  
441 2019. **185**: p. 1154-1162.
- 442 13. Huo, E., et al., *Experimental and theoretical studies on the thermal stability and*  
443 *decomposition mechanism of HFO-1336mzz(Z) with POE lubricant*. Journal of  
444 Analytical and Applied Pyrolysis, 2020. **147**.
- 445 14. Wang, Y., et al., *Theoretical and experimental studies on the thermal*

- 446 *decomposition and fire-extinguishing performance of*  
447 *cis-1,1,1,4,4,4-hexafluoro-2-butene.* International Journal of Quantum  
448 Chemistry, 2020. **120**(9).
- 449 15. Zhang, H., et al., *Thermal Decomposition Mechanism and Fire-Extinguishing*  
450 *Performance of trans-1,1,1,4,4,4-Hexafluoro-2-butene: A Potential Candidate*  
451 *for Halon Substitutes.* Journal of Physical Chemistry A, 2020. **124**(28): p.  
452 5944-5953.
- 453 16. Xin, L., et al., *Thermal decomposition mechanism of some hydrocarbons by*  
454 *ReaxFF-based molecular dynamics and density functional theory study.* Fuel,  
455 2020. **275**.
- 456 17. Cao, Y., et al., *Influence of water on HFO-1234yf oxidation pyrolysis via*  
457 *ReaxFF molecular dynamics simulation.* Molecular Physics, 2019. **117**(13): p.  
458 1768-1780.
- 459 18. Wang, X., et al., *Suppression of propane cup-burner flame with*  
460 *HFO-1336mzz(Z) and its thermal stability study.* Thermochemica Acta, 2020.  
461 **683**.
- 462 19. Zhang, H., et al., *Mechanism of thermal decomposition of HFO-1234yf by DFT*  
463 *study.* International Journal of Refrigeration-Revue Internationale Du Froid,  
464 2017. **74**: p. 399-411.
- 465 20. Huang, J., et al., *A density functional theory study on formation mechanism of*  
466 *CO, CO<sub>2</sub> and CH<sub>4</sub> in pyrolysis of lignin.* Computational and Theoretical  
467 Chemistry, 2014. **1045**: p. 1-9.
- 468 21. Navarro-Esbri, J., et al., *Experimental study of an Organic Rankine Cycle with*  
469 *HFO-1336mzz-Z as a low global warming potential working fluid for*  
470 *micro-scale low temperature applications.* Energy, 2017. **133**: p. 79-89.
- 471 22. Zheng, M., et al., *Initial Chemical Reaction Simulation of Coal Pyrolysis via*  
472 *ReaxFF Molecular Dynamics.* Energy & Fuels, 2013. **27**(6): p. 2942-2951.
- 473 23. Beste, A., *ReaxFF Study of the Oxidation of Softwood Lignin in View of Carbon*  
474 *Fiber Production.* Energy & Fuels, 2014. **28**(11): p. 7007-7013.
- 475 24. Ren, C., et al., *Decomposition mechanism scenarios of CL-20 co-crystals*  
476 *revealed by ReaxFF molecular dynamics: similarities and differences.* Phys  
477 Chem Chem Phys, 2020. **22**(5): p. 2827-2840.
- 478 25. van Duin, A.C.T., et al., *ReaxFF: A reactive force field for hydrocarbons.*  
479 Journal of Physical Chemistry A, 2001. **105**(41): p. 9396-9409.
- 480 26. Chenoweth, K., A.C.T. van Duin, and W.A. Goddard, III, *ReaxFF reactive force*  
481 *field for molecular dynamics simulations of hydrocarbon oxidation.* Journal of  
482 Physical Chemistry A, 2008. **112**(5): p. 1040-1053.
- 483 27. Ashraf, C., et al., *Pyrolysis of binary fuel mixtures at supercritical conditions: A*  
484 *ReaxFF molecular dynamics study.* Fuel, 2019. **235**: p. 194-207.
- 485 28. Sorensen, M.R. and A.F. Voter, *Temperature-accelerated dynamics for*  
486 *simulation of infrequent events.* Journal of Chemical Physics, 2000. **112**(21): p.  
487 9599-9606.

- 488 29. Cao, Y., et al., *Thermal decomposition of HFO-1234yf through ReaxFF*  
489 *molecular dynamics simulation*. Applied Thermal Engineering, 2017. **126**: p.  
490 330-338.
- 491 30. Gaussian., R.A., Frisch, G.W.T.M.J., Schlegel, H.B., Scuseria, G.E., Robb,  
492 J.R.C.M.A., Scalmani, G., Barone, V. Mennucci, B., Petersson, H.N.G.A.,  
493 Caricato, M., Li, X., Hratchian, H.P., Izmaylov, J.B.A.F., Zheng, G.,  
494 Sonnenberg, J.L., Hada, M., Ehara, K.T.M., Fukuda, R., Hasegawa, J., Ishida,  
495 M., Nakajima, T., Honda, O.K.Y., Nakai, H., Vreven, T., Montgomery, J.A. Jr.,  
496 Peralta, F.O.J.E., Bearpark, M., Heyd, J.J., Brothers, E., Kudin, V.N.S.K.N.,  
497 Kobayashi, R., Normand, J., Raghavachari, A.R.K., Burant, J.C., Iyengar, S.S.,  
498 Tomasi, J., Cossi, N.R.M., Millam, J.M., Klene, M., Knox, J.E., Cross, J.B.,  
499 Bakken, C.A.V., Jaramillo, J., Gomperts, R., Stratmann, R.E., Yazyev,  
500 A .J.A .O., Cammi, R., Pomelli, C., Ochterski, J.W., Martin, K.M.R.L.,  
501 Zakrzewski, V.G., Voth, G.A., Sal-vador, J.J.D.P., Dapprich, S., Daniels, A.D.,  
502 Farkas, J.B.F.O., Ortiz, J.V., Cioslowski, J., Fox, D.J., Gaussian 09, Gaussian,  
503 Inc, Wallingford, CT, 2009.
- 504 31. Islam, M.M., V.S. Bryantsev, and A.C.T. van Dian, *ReaxFF Reactive Force*  
505 *Field Simulations on the Influence of Teflon on Electrolyte Decomposition*  
506 *during Li/SWCNT Anode Discharge in Lithium-Sulfur Batteries*. Journal of the  
507 Electrochemical Society, 2014. **161**(8): p. E3009-E3014.
- 508

**Table 1**

Initial densities and ensemble of ReaxFF simulation about DR-2.

	<b>Molecules</b>	<b>Initial density ( <math>\rho / g \cdot cm^{-3}</math> )</b>	<b>Ensemble</b>
Ref.[9]	50 DR-2	1.3595	NVT
Ref.[11]	150 DR-2 + 450 O <sub>2</sub> (1)	0.015 (1)	NVT
	75 DR-2 + 450 O <sub>2</sub> (2)		
	300 DR-2 + 450 O <sub>2</sub> (3)		
Ref.[12]	150 DR-2 + 450 O <sub>2</sub> (1)	0.015	NVT
	150 DR-2 + 450 O <sub>2</sub> +37 H <sub>2</sub> O (2)		
	150 DR-2 + 450 O <sub>2</sub> +75 H <sub>2</sub> O (3)		
	150 DR-2 + 450 O <sub>2</sub> +112 H <sub>2</sub> O (4)		
	150 DR-2 + 450 O <sub>2</sub> +150 H <sub>2</sub> O (5)		
This work	100 DR-2 + 50 O <sub>2</sub> (1)	0.00538 (1)	NVT
	45 DR-2 (2)	1.36 (2-3)	
	45 DR-2 +5 O <sub>2</sub> (3)		